Modeling white matter microstructure

Tanguy Duval, MSc[a]
Nikola Stikov, PhD[a,b]
Julien Cohen-Adad, PhD[a,c]

[a] NeuroPoly Lab, Institute of Biomedical Engineering, Polytechnique Montreal, Montreal, QC, Canada
[b] Montreal Heart Institute, Montreal, QC, Canada
[c] Functional Neuroimaging Unit, CRIUGM, Université de Montréal, Montreal, QC, Canada

Correspondence to: Julien Cohen-Adad
E-mail: jcohen@polymtl.ca

Summary

Quantitative magnetic resonance imaging can be combined with advanced biophysical models to measure microstructural features of white matter. Non-invasive microstructural imaging has the potential to revolutionize neuroscience, and acquiring these measures in clinically feasible times would greatly improve patient monitoring and clinical studies of drug efficacy. However, a good understanding of microstructural imaging techniques is essential to set realistic expectations and to prevent over-interpretation of results. This review explains the methodology behind microstructural modeling and imaging, and gives an overview of the breakthroughs and challenges associated with it.

KEY WORDS: diffusion, g-ratio, microstructure, MRI, myelin imaging, white matter

Introduction

Magnetic resonance imaging (MRI) is an attractive, non-invasive modality that can provide information about the integrity of the central nervous system (CNS) at a resolution in the order of $1mm^3$. To produce an image, an MRI scanner excites the magnetic moments of hydrogen atoms in water molecules, or spins, using radio waves. The excited spins will then re-emit a radio wave that is characterized by the water density as well as the time constants T1 and T2, which reflect the tissue chemical environment, thereby providing the image contrast. Thanks to its high sensitivity to soft tissue (not shown by X-ray), conventional MRI can distinguish different structures and detect lesions (e.g. inflammation, scar tissue, low-grade tumors). This good sensitivity is limited, however, by a lack of specificity, and it is usually difficult to establish a relationship between lesion activity observed by MRI and clinical score and patient prognosis (Rovira et al., 2013). However, the potential of MRI goes far beyond its capacity to provide simple contrast between tissues. By varying, in a controlled fashion, the excitation and the dephasing of the spins that produce the magnetic resonance (MR) signal, researchers are able to measure several chemical and physical properties, such as the local change in oxygenation in functional MRI, the diffusion profile of water molecules in diffusion MRI, and the proportion of different macromolecules or metabolites (e.g. myelin lipids or iron) in relaxometry, magnetization transfer and MR spectrometry. Instead of providing arbitrary numbers, these different MRI modalities can be calibrated in order to extract quantitative metrics, reproducible across sites (with different brands of scanner and with different coils). These techniques are commonly called “quantitative MRI” (Cohen-Adad and Wheeler-Kingshott, 2014; Tofts P, 2003). While many quantitative MRI metrics, such as T1 or fractional anisotropy (FA) from diffusion MRI, are now widely used by clinicians, they are still difficult to interpret, notably because they lack specificity . To further understand how the complex chemical environment influences these quantitative metrics, researchers have proposed to take up the challenge of modeling mathematically the relationship between the white matter microstructure and the generated MRI signal. Using the resulting models, they can extract meaningful numbers, such as the size and density of tissue fibers, the concentration of myelin or iron within a voxel, and the thickness of the myelin sheath surrounding the axons. These microstructural metrics are usually called “model-based quantitative metrics” as opposed to “physical quantitative metrics” (e.g. T1 or ADC, i.e. apparent diffusion coefficient). The ability to measure quantitatively many different properties with a single system allows comprehensive characterization of white matter tissue, from its composition to its microstructure. While the different information is usually exploited separately, complementary MRI metrics can also be combined to extract complete and specific information about the tissue, which can help with diagnosis and prognosis of neurodegenerative disorders.

In practice, quantitative MRI metrics are extracted by acquiring multiple images of the same modality (e.g. diffusion MRI), using different acquisition parameters (e.g. diffusion time). By modeling the signal change as a function of these acquisition parameters, one can extract quantitative information. In this review, we focus on model-based quantitative MRI metrics (which exclude physical quantitative metrics) and describe the methodology for modeling the white matter microstructure and the associated MRI signal. The challenges and limits of these techniques will also be addressed.

White matter microstructure

To model the MRI signal it is essential to have sufficient knowledge of the underlying tissue microstructure. For instance, precise knowledge of the volume fraction of a certain water component makes it easier to understand its contribution to the MRI signal: the bigger this compo-

nent is, the more it contributes to the signal (weighted by the T1 and T2 relaxations).

Figure 1 shows an example of white matter electron microscopy (a) along with a schematic drawing of white matter microstructure (b). The white matter is composed of four main components: neurons, glial cells (e.g. astrocytes, microglia, oligodendrocytes), the extracellular space, and blood vessels.

Neurons can be subdivided into fibers, cell bodies and dendrites. In the white matter, we observe very few neuronal bodies and dendrites[1], and the majority of the space is occupied by neuronal fibers (~60%) (Mottershead et al., 2003; Perge et al., 2009; Stikov et al., 2015a). The extracellular space constitutes about 20% of the volume (Bourne, 2012; Syková and Nicholson, 2008), blood vessels constitute less than 3% (Syková and Nicholson, 2008), while the rest of the volume is occupied by glial cells. 70 to 95% of the nerve fibers are enveloped by a myelin sheath (Biedenbach et al., 1986; Liewald et al., 2014) (myelin is responsible for the white appearance of the white matter). Furthermore, myelinated fibers are, on average, much larger than unmyelinated fibers (20 to 50% larger) (Biedenbach et al., 1986; FitzGibbon and Nestorovski, 2013), with the result that the majority of the space is occupied by myelinated fibers. The term fiber refers to the axon plus its myelin

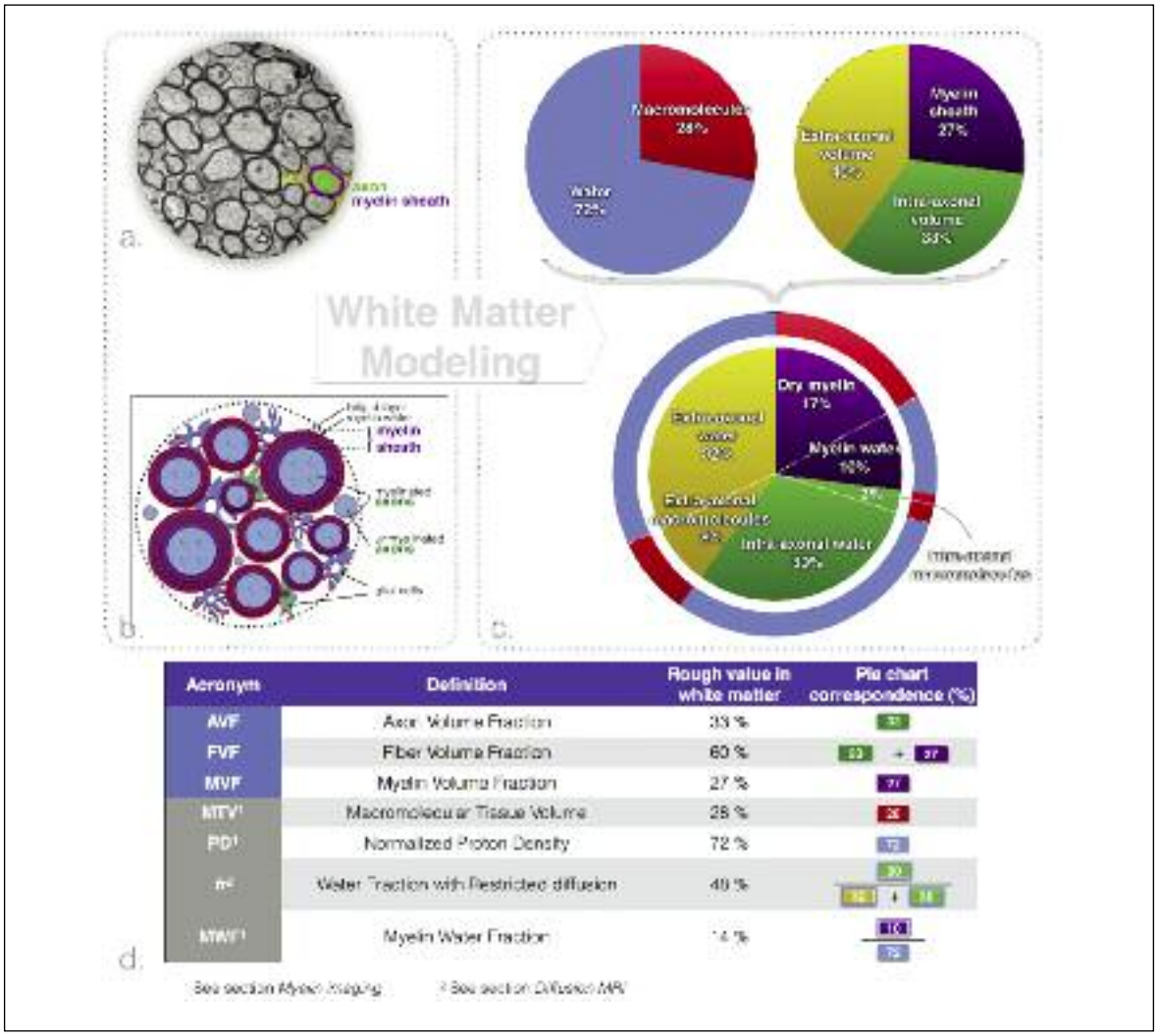

Figure 1 - Modeling of white matter tissue.

a. Transmission electron microscopy of an axial slice of white matter fiber bundles extracted from the corpus callosum of a mouse (West et al., 2016a). b. Schematic representation of the white matter. c. Proportions of the different white matter tissue components. The top left pie chart divides white matter into two general components: water (blue) (the component that produces the MRI signal) and lipids/macromolecules (red). The top right pie chart divides white matter into three spaces (used in diffusion and myelin imaging models): the myelin sheath (purple), the extra-axonal volume (yellow) and the intra-axonal volume (green). The bottom pie chart subdivides these three spaces into water and lipid/macromolecular content. d. Definitions of most commonly used MRI (gray boxes) and tissue modeling (light blue boxes) metrics and their rough values.

[1] The soma to glial cell ratio is 1:15 in white matter versus 1:1 in gray matter (Azevedo et al., 2009), while glial cell density is similar in white and gray matter (Herculano-Houzel, 2014).

sheath. About 33%[2] of the white matter volume is composed of axons (Nilsson et al., 2013; Perge et al., 2009). All these components are highly hydrated [the water content of white matter is ~72% (Lajtha, 2013; Tofts PS, 2003)]. The axoplasm is composed largely of water (87%) and contains 2.5% proteins (assessed in squid giant axons) (Johansen-Berg and Behrens, 2013; Adelmann et al., 2013). Glial cells and blood vessels are composed of ~80% water (Shepherd, 2006); The extracellular space contains mainly fluid, supplemented by long macromolecules that constitute the extracellular matrix (Syková and Nicholson, 2008); only the myelin sheath presents a relatively low water content of 40% (Morell and Quarles, 1999; Norton and Cammer, 1984). In fact, 50 to 60% of the dry tissue weight in white matter is myelin (Norton and Autilio, 1966), and this proportion reaches 75% in peripheral nerves (O'Brien and Sampson, 1965).

Glial cell density is very constant in the brain [~10^5 cells/mm^3 (Herculano-Houzel, 2014)], suggesting a homogeneous contribution of glial cells to the MRI signal strength. Axon density, however, varies greatly (10^4 to 105/mm^3) due to large differences in mean axon diameter between regions (Herculano-Houzel, 2014).

Axons are myelinated by oligodendrocytes (one oligodendrocyte for up to 50 axons [(Baumann and Pham-Dinh, 2001)], which wrap multiple layers of myelin around the axons until the ratio of the inner to the outer diameter of the fiber, called the g-ratio, achieves an optimal value of around 0.77 (Chomiak and Hu, 2009). The myelin sheath is thus a succession of impermeable bilipid layers, separated by layers of water (myelin water). In adults, the myelin sheath occupies approximately 25–30% of the white matter volume (Mottershead et al., 2003; Perge et al., 2009; Stikov et al., 2015a). The function of the myelin layers is to improve the speed of propagation of action potentials by inhibiting ionic exchanges between the intra- and the extra-axonal space. Instead, these exchanges mostly take place at the regularly spaced nodes of Ranvier. These nodes are ~2μm long and spaced ~1 mm apart (depending on the axon diameter), and thus constitute only 0.2% of the axon surface (Giuliodori and DiCarlo, 2004). This anatomical feature explains why water diffuses preferentially along the nerve fibers (about four times faster than perpendicular to the fibers), as observed in diffusion tensor imaging experiments (Alexander et al., 2007), and also explains the presence of a slow diffusion component perpendicular to the fibers that is attributed to water "trapped" inside the axons (Clark and Le Bihan, 2000).

Nuclear magnetic resonance (NMR) experiments have established that the exchange rate between the intra- and the extra-axonal space is ~600 ms (Duong et al., 1998; Meier et al., 2003; Nilsson et al., 2013), an order of magnitude longer than the typical diffusion time used in diffusion MRI. Axons can thus be considered impermeable to water in diffusion MRI models. As for glial cells, their membrane is more permeable thanks to the presence of aquaporin pores on their surface (Arciénega et al., 2010; Nielsen et al., 1997). This is confirmed by the greater restriction (50% decrease of the diffusion coefficient) of water molecules after deactivation of these aquaporin pores (Badaut et al., 2011), and the appearance of a new water compartment, isotropically restricted, in fixed tissue (~30% of the MRI-visible water) (Panagiotaki et al., 2012), much larger than in *in vivo* tissue (Ferizi et al., 2014). Similarly to glial cells, water molecules in blood vessels are not restricted, because of the rapid exchange (exchange rate of 15-30 ms) with the extracellular space and the glial cells (Johansen-Berg and Behrens, 2013).

The pie charts in figure 1 summarize the above information and give rough estimates of the volume fraction of the different constituents of white matter, values that are particularly useful in myelin imaging.

Quantitative MRI modalities

In this section, important quantitative MRI modalities are briefly presented, focusing on the fundamental physics that allows the methodology to retrieve meaningful measures of tissue microstructure. This section also highlights the advantages of these metrics compared to conventional MRI and clarifies the limitations in their interpretation.

Diffusion MRI

Theory

A popular modality for assessing tissue microstructure is diffusion MRI. Diffusion MRI takes advantage of the diffusion of water molecules to probe the microenvironment. Just as the diffusion of a drop of ink on a fibrous tissue reveals the direction of the microscopic fibers that compose that tissue (Fig. 2), diffusion MRI reveals the direction of the fibers that compose the white matter tissue, a technique called diffusion tensor imaging (DTI). In each voxel and in multiple directions, the diffusion of water molecules is measured thanks to an equation that relates MRI signal reduction to the diffusion rate of water molecules (Stejskal and Tanner, 1965) (see next paragraph). If the diffusion is modeled in 2D, it can be described by an ellipse, as illustrated with the drop of ink (Fig. 2). In 3D the diffusion can be described by a tensor (a 3x3 symmetric matrix with six parameters), therefore at least six diffusion-weighted MR images need to be acquired to resolve its shape. This can be done for each individual voxel in the MRI acquisition. This principle can be pushed further to measure the amount of water trapped inside the myelinated fibers, and the size distribution of these fibers (Assaf et al., 2008). Indeed, these water molecules present restricted diffusion and result in a small MRI signal decrease. Although models exist for different tissues (e.g. kidney cells, gray matter), the majority of the models have been adapted to white matter tissue, because white matter presents fewer dendrites and many myelinated fibers in relatively coherent orientations.

[2] Note that an axon volume fraction of 33% and a fiber volume fraction of 60% leads to a g-ratio of $\sqrt{(33/60)}=0.74$, which is close to the optimal value of 0.77 as mentioned in Chomiak and Hu (2009).

Diffusion encoding in MRI is performed through the dephasing and rephasing of the spins using magnetic field gradients, referred to in this paper as "diffusion gradients". The standard diffusion protocol is the pulsed-gradient spin echo sequence, which is composed of two diffusion gradients characterized by three parameters: their duration δ, amplitude G, and separation Δ (Fig. 3). The relationship between diffusion gradients and MRI signal was first expressed by Stejskal and Tanner (1965) assuming a Gaussian diffusion:

$$S = S_0 e^{-bD}$$

where S_0 represents the MR signal when no diffusion encoding is applied (i.e. $b = 0$), $b = (\gamma\delta G)^2 \cdot (\Delta - \delta/3)$ (s/mm^2), and D (mm^2/s) is the diffusion coefficient in the direction of the diffusion gradients.

Advanced modeling

The MR model for Gaussian diffusion is thus characterized by a single parameter *b* instead of three (Δ, δ, and G). This equation can be validated experimentally by measuring the evolution of the MR signal in water for different combinations of Δ, δ, and G (Fig. 4). However, the same experiment in the white matter (with diffusion gradient directions perpendicular to the main axis of the axons) shows that: i) a single exponential is not sufficient to model the MR signal decay as a function of the *b*-value, and ii) the MR signal is not a function of the *b*-value only (see figure 4). The first observation led to the development of the models with multiple compartments, a slow diffusion compartment that corresponds to the trapped water (within myelinated axons for instance), and a fast diffusion compartment that corresponds to the water that is diffusing in the extracellular matrix or is in active exchange with glial cells (e.g. astrocytes via the aquaporin pores). The second observation (signal is not dependent only on the *b*-value) requires the use of non-Gaussian diffusion equations to model the slow compartment. The equation of restricted diffusion within cylinders of known diameter (Wang et al., 1995) correctly models this non-Gaussianity of diffusion in white matter (Alexander et al., 2010; Assaf and Basser, 2005; Avram et al., 2004; Ferizi et al., 2014, 2015; Nilsson et al., 2013; Panagiotaki et al., 2012; Zhang et al., 2012). This non-Gaussian compartment is usually attributed to the water restricted in myelinated fibers. Although the extra-axonal compartment is a complex structure, assuming Gaussian diffusion in this compartment correctly models the MRI signal (Alexander et al., 2010; Assaf and Basser, 2005; Ferizi et al., 2015; Nilsson et al., 2013; Zhang et al., 2012), probably due to the good permeability of the membranes (see section "White matter microstructure"), although this assumption can be refined when varying the diffusion time (Burcaw et al., 2015).

While Gaussian diffusion, notably used in DTI experiments, is a good approximation at low *b*-values (typically $b = 1500$ s/mm^2) for a fixed diffusion time, advanced models, such as those from the previous paragraph, are necessary for larger *b*-values or in experiments with various diffusion times in order to get measurements (e.g. diffusion coefficients) that are independent of the acquisition protocol (e.g. choice of *b*-values and diffusion times). Another asset of these more advanced models is their robustness to partial volume effects or contamination with cerebrospinal fluid (CSF). Not accounting for these effects leads to abnormally low values of FA, for

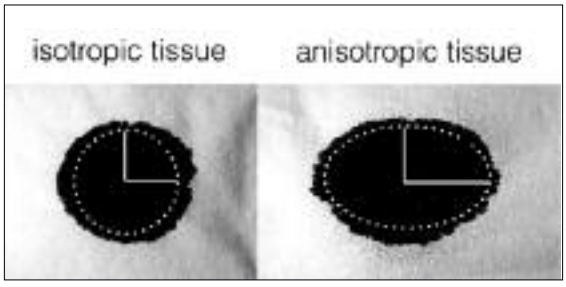

Figure 2 - Diffusion reveals the underlying microstructure of the tissue.

The diffusion of a drop of ink on isotropic (left) or anisotropic (right) fibrous tissue is Gaussian and can be modeled with an ellipse. The main axis of this ellipse (horizontal axis in this case) defines the main direction of the fibers that form the tissue. The ratio between the main and the secondary axis defines the degree of anisotropy of the paper. Similarly, diffusion in the white matter tissue is modeled with an ellipsoid in diffusion tensor imaging experiments. This figure was inspired by Dr Gordon Kindlmann (University of Chicago).

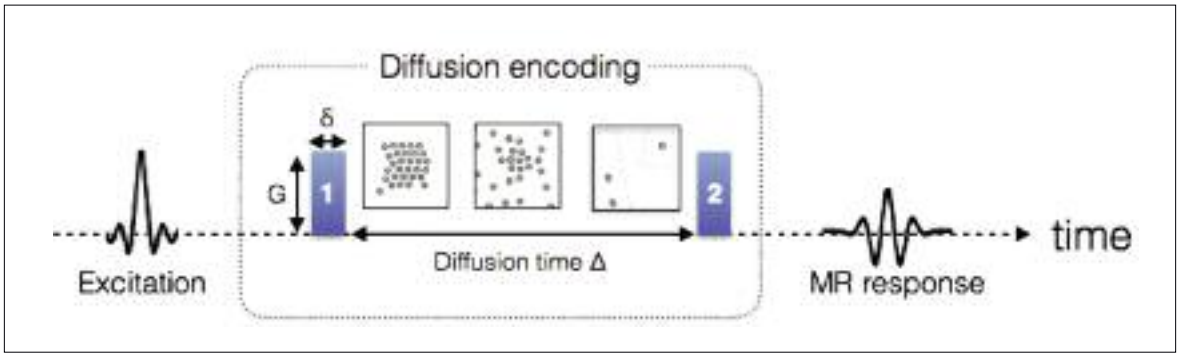

Figure 3 - Timeline for encoding the diffusion of the water molecules in MRI.

Just after being excited, the position of each molecule is tagged based on the phase of its spins, by applying gradient #1 (parametrized by its strength G and duration δ). During a time Δ, the spins (illustrated by small circles) move (due to Brownian motion or convection). The longer the time Δ is, the further the molecules can move. A second and identical gradient is applied to quantify this displacement through a signal loss in the MR response.

instance at the periphery of the white matter tissue, notably close to ventricles or at the periphery of the spinal cord, even if the tissue is healthy.
These models can thus be used to describe tissue microstructure. The relative proportion between the restricted water trapped inside axons and the water presenting Gaussian diffusion outside the axons can be retrieved (metric *fr* in Fig. 1), and some models also feature the orientation dispersion or the permeability of the myelin sheath (Clark and Le Bihan, 2000; Nilsson et al., 2012, 2013; Panagiotaki et al., 2012; Zhang et al., 2012). Some of these parameters can be measured robustly only with a system that can achieve very high gradient strengths, while others are adapted for clinical scanners.

Myelin imaging

In one important field of MRI research, the aim is to measure the myelin content within a tissue. Myelin imaging is particularly interesting in neurodegenerative diseases, as well as in several neurological disorders (e.g. autism, schizophrenia), because of the presence of demyelination or abnormal myelination of neuronal fibers (Fields, 2008). Unfortunately, measuring the signal directly from myelin is challenging due to the ultrashort myelin relaxation times (T2~10 μs), and because the signal from myelin gets lost in the strong water signal. Although some groups showed very promising results of direct myelin imaging in humans *in vivo* (Sheth et al., 2016), such techniques are very recent and further validation is required. Instead of detecting the myelin directly, researchers have developed strategies to retrieve quantitative metrics that correlate with absolute myelin content (or myelin volume fraction, MVF) from the water signal. As a consequence, it should be kept in mind that the term myelin imaging can be misleading. Indeed, these techniques provide quantitative metrics that need to be calibrated, assuming a linear relationship with MVF, in order to retrieve the true myelin content. Usually, the coefficients of this linear relationship are not perfectly known and might change in pathology (e.g. effect of the non-compact myelin sheath in multi-component T2 experiments). Also, some of these techniques are sensitive to all lipids and macromolecules in general (e.g. magnetization transfer) and not only to myelin. Different physical properties have been used to obtain metrics sensitive to myelin content.

Magnetization transfer

One strategy is to take advantage of the phenomenon called magnetization transfer (MT) (Wolff and Balaban, 1989), where the hydrogen spins bound to macromolecules, once excited by a dedicated radiofrequency pulse, transfer a part of their energy to the neighboring free water spins. The more the macromolecules present in the voxel, the greater the number of free water spins excited via this phenomenon, which impacts on the MR signal. The most common metric utilizing this phenomenon is the magnetization transfer ratio (MTR), which has been shown to correlate with myelin content (Schmierer et al., 2004), but also with other properties such as the T1 relaxation time (Henkelman et al., 2001). A particularly interesting improvement of MTR is the saturated magnetization transfer metric (MTsat) (Helms et al., 2008): MTsat decouples MTR from T1, but is still protocol-dependent. In order to derive truly quantitative metrics from the MT phenomenon, researchers proposed modeling it in white matter and introduced equations of the MR signal change as a function of acquisition parameters (e.g. frequency or power of the radiofrequency pulse that excites the macromolecules), a technique called quantitative MT (qMT) (Henkelman et al., 1993). While comprehensive models are theoretically able to quantify myelin content (Harrison et al., 1995), fitted parameters are too unstable to be estimated *in vivo* (Levesque and Pike, 2009). Alternatively, qMT extracts the volume fraction of all macromolecules in a voxel (i.e. not only myelin, but also membranes of other cells and organelles).

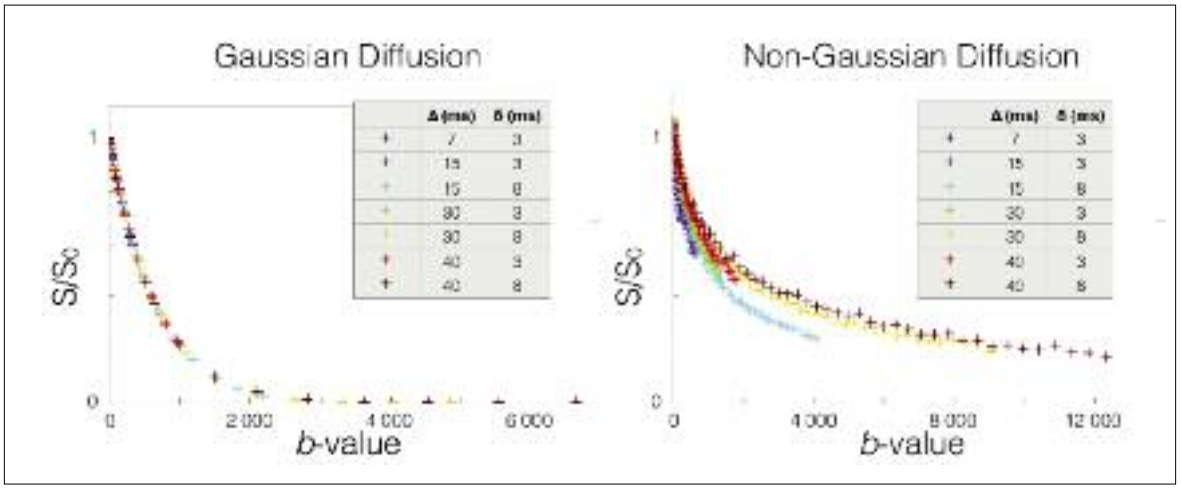

Figure 4 - MRI signal as a function of *b*-value in voxels presenting Gaussian (left) or non-Gaussian (right) diffusion of water molecules.
While conventional diffusion MRI assumes Gaussian diffusion characterized by dependence on the *b*-value only, diffusion perpendicular to neuronal fibers (right) is non-Gaussian, which allows the extraction of additional microstructural information such as axon diameter.

Myelin water fraction

Another strategy is to exploit the relationship between myelin content and spin relaxometry. Indeed, the water contained in the myelin sheath (myelin water amounts to approximately 40% of the myelin volume) presents a very short T2 relaxation time compared with the rest of the water molecules. By measuring the amount of water with a short T2 relaxation time, it is possible to measure the myelin water fraction (MWF) (MacKay et al., 1994). It is also possible to infer the myelin volume fraction from the MWF if we assume that 40% of myelin water is in the myelin sheath. While initial implementations of this technique suffered from high noise level, new acquisition strategies and models have been developed to obtain higher quality images and to make this technique usable for clinical studies (Deoni et al., 2008; Oh et al., 2013; Prasloski et al., 2012). Note that T1 relaxation time can also be used for myelin imaging as proposed by Stüber et al. (2014), keeping in mind that T1 is potentially biased by axon diameter (Harkins et al., 2016).

Normalized proton density

Another relevant metric for microstructure modeling is the measurement of the water content obtained using normalized proton density (PD) mapping (Tofts PS, 2003; Volz et al., 2012). The complement of this metric is the non-water volume; this provides a measure of the macromolecular tissue volume (MTV), which includes lipids (Mezer et al., 2013). While all raw MR images are PD weighted, obtaining quantitative measurement of the water content requires challenging corrections of coil excitation (B1+) and sensitivity (B1−) profiles, as well as a calibration of the signal with relatively pure water (e.g. CSF) (Mezer et al., 2013; Tofts PS, 2003; Volz et al., 2012). With a good correction and calibration pipeline, water content can be measured precisely and with high reproducibility in the brain (Mezer et al., 2013).

Multimodal MRI

Thanks to ongoing improvements in acquisition sequences, protocols and hardware, it is now possible to obtain quantitative maps rapidly (in less than 10 min). By obtaining multiple quantitative MRI maps in a reasonable time it is possible to get complementary information on the tissue microstructure. The different metrics can be combined using models to derive more robust and relevant quantitative metrics, commonly called multimodal or multi-parametric measurements. One example is the computation of the fiber g-ratio, defined as the ratio of the axon caliber to the fiber caliber (axon plus myelin). The g-ratio can be computed by combining the restricted water fraction (*fr*) obtained with quantitative diffusion MRI, and the MVF obtained with myelin imaging. Taken independently, both *fr* and MVF are affected by CSF contamination or edema. In the computation of the g-ratio, these effects are compensated for; this simplifies the interpretation in case of demyelination, and is expected to improve the specificity of the technique to myelin sheath thickness.
The recent development of MR fingerprinting also offers interesting ways to obtain multi-parametric maps in a rapid manner (Ma et al., 2013), although further validation is still required before these techniques can be applied to pathological cases.

Challenges

In addition to practical and technical challenges, quantitative MRI presents fundamental challenges that make the modeling and interpretation of quantitative MRI results difficult.

Inferring the microscopic from the macroscopic

The signal is an average of many micro- and nanoscopic processes occurring over space (one voxel is composed of millions of magnetic spins) and time (usually in the order of milliseconds). The diffusion, for instance, is due to the Brownian movement and convection of water molecules within cells, between cells and through membrane aquaporin pores. Although very complex at nanoscopic scale, these chaotic displacements of water molecules can be described through probability functions [e.g. Gaussian in free water (Einstein, 1956)] that are highly reproducible on a macroscopic scale, and can therefore be modeled. But these probability functions also depend on the microscopic structure of the tissue (e.g. size of the cells and direction of the fibers), which hinders or restricts the global diffusion and thus modifies the MRI signal. Explaining the macroscopic features from the micro- and nanoscopic processes requires the isolation of the main effects from the negligible ones, a task that is particularly difficult because i) many of the parameters involved are related to the MRI acquisition (e.g. magnetic gradient strength, duration, delays) and physics (e.g. diffusion coefficients, membrane permeabilities, exchange rates); ii) the precision of the measurements, hardware capability and experiment duration are limited, and iii) the observed signal usually shows a simple behavior (e.g. bi-exponential) with only subtle changes.

Choosing the right model

Due to this difficulty in relating the macroscopic to the microscopic, many models have been developed for each MRI modality. While most diffusion models share the same approach (i.e., they are based on a mixture of free, hindered and restricted water compartments), they usually propose to take into account additional effects or to make additional simplifications and assumptions. Choosing the right model is not straightforward and multiple criteria need to be taken into account. The complexity of the model, which can be defined by the number of parameters to fit, is one important criterion; while the most complex models are supposedly more accurate and specific, they produce less precise metrics with worse image quality, and thus cannot detect a subtle change in tissue integrity.
On the other hand, simple models produce metrics that are harder to interpret because of the difficulty in decoupling the contributions from multiple sources. Another criterion for choosing the right model is the targeted tissue. Indeed, in the majority of the white matter, the large dispersion of orientation (and crossing) of the fibers needs to be taken into account in the diffusion model (via additional parameters). Zhang et al. (2012) proposed a popular model called NODDI that can quantify this dispersion of orientation as well as the intra-axonal volume. However, this aspect can be neglected

(which simplifies the modeling) in the spinal cord white matter where there is good coherence of orientation (Grussu et al., 2016).
Choosing the right model also goes hand in hand with deciding the acquisition strategy: instead of building very complex models that would work with any acquisition protocol, another interesting strategy is to adapt the acquisition in order to simplify the modeling. For instance, acquiring diffusion data only in one direction perpendicular to the direction of the fibers (in tissues with good coherence of orientation) allows simpler modeling than a complete 3D acquisition, and thus the extraction of more robust metrics with shorter protocols. Another example is the choice of diffusion time in the protocol: the longer the diffusion time, the more hindered the diffusion in the extra-axonal compartment (Burcaw et al., 2015). Acquisition protocols that have only long diffusion times will thus be modeled differently from those consisting only of short durations. Some groups even proposed changing the acquisition paradigm: oscillating instead of pulsed magnetic gradients have been used successfully to encode the diffusion (Lundell et al., 2015; Shemesh et al., 2015); additional preparatory pulses have been used in myelin imaging to cancel the signal from free water protons (VISTA) (Oh et al., 2013).

Validating the models

Testing and validating the different models requires a good ground truth, which is hard to get. The comparison of the MRI signal with histology, as well as the fabrication of realistic and well-controlled synthetic phantoms is an active field of research in microstructural imaging. Histology is technically complex due to tissue deterioration during the preparation stages (e.g. fixation, staining, slicing) and it is limited due to the many coupled variables that cannot be controlled independently. While histology is a great method for demonstrating the sensitivity to a particular microstructural feature, it cannot easily be used to show the specificity. Indeed, microstructural properties (g-ratio, T1, absolute myelin content, water content, axon diameter) generally correlate with each other. Hence, assessing with confidence the specificity of each individual metric is an inherently ill-posed problem.
The issue of validation from *ex vivo* data is further complicated by the difficulty in generating, from histology, ground truth data that match the resolution of MRI: within a single MRI voxel there lie thousands of axons, which need to be individually labeled in order to retrieve aggregated ground truth metrics such as axon diameter and myelin. Fortunately, recent efforts in open-source software[3] for automatic axon and myelin segmentation (Zaimi et al., 2016) will make it easier for researchers to use large-scale histology and validate the relationship of their metric with the desired microstructural feature. Although numerical and synthetic phantoms allow for better-controlled experiments, this approach needs to be complemented with more realistic white matter tissue. In summary, there is no perfect validation method and the research community relies on the accumulation of evidence from diverse approaches to validate quantitative MRI methods.

Translating the models to the damaged tissue

Tissue characteristics can change drastically in pathology. The proliferation of microglia, inflammation, the presence of axonal debris, or the constitution of a glial scar in nervous tissue limit the validity of some assumptions used in models [e.g. impermeability of the myelin sheath in demyelination, unrestricted diffusion in the extra-axonal compartment (Syková et al., 1999)]. Choosing a model that is robust to all pathological cases is one of the biggest challenges of quantitative MRI.

Performance of quantitative MRI metrics

Quantitative MRI has seen many improvements thanks to better acquisition strategies (Deoni et al., 2003; Marques et al., 2010; Oh et al., 2013; Prasloski et al., 2012; Van et al., 2014), optimized experimental designs (Alexander, 2008), more robust models (Zhang et al., 2012), and advanced data processing, such as faster and more stable equation solvers (Daducci et al., 2015; Sepehrband et al., 2016). On top of that, acquisition time, noise level and image artifacts (e.g. sensitivity to movement) have been improved thanks to improvements in hardware, in terms of field and gradient strength, coils and sequences (e.g. parallel imaging, simultaneous multislice excitation, reduced field of view). By combining all these improvements, the quantitative MRI metrics cited in previous sections can provide high-quality maps, with image quality similar to that of conventional MRI images, in just a couple of minutes. Beyond these improvements in acquisition time and image quality, quantitative MRI also requires accurate and reproducible ways of extracting the values in specific regions, a task facilitated by the development of automatic and robust segmentation, registration and metric extraction software and pipelines (Dupont et al., 2016; Vollmar et al., 2010). Unfortunately integrating all these improvements is difficult and time-consuming; in practice, basic or unoptimized methods are always used at some point, which leaves space for even better results in the future.

Qualitative assessment

One approach to estimate the sensitivity and precision of a quantitative metric is to qualitatively assess the level of noise and detail in the maps. In the latest implementations, model-based diffusion MRI metrics can produce highly detailed maps with high contrast-to-noise ratio (Daducci et al., 2015). Although MWF mapping was particularly noisy when it was first introduced (MacKay et al., 1994), relatively good quality MWF maps can now be obtained rapidly (Deoni et al., 2008; Oh et al., 2013; Prasloski et al., 2012). qMT generates maps with similar noise level as MWF (depending on acquisition time), but with particularly small contrast in the white matter (Dula et al., 2010; Levesque et al., 2010). Proton density maps are highly detailed with relatively good quality and correlate with qMT and MWF (Mezer et al., 2013).

[3] https://github.com/neuropoly/axonseg

Reproducibility

The reproducibility of quantitative metrics is usually assessed by the coefficient of variation (CoV) and/or the voxel-wise Pearson correlation coefficient (r) in scan-rescan experiments of the same subject at two different time points (the subject is removed from the scanner between scans).

Most model-based quantitative metrics have a good CoV (<10%). These include *fr* (Grussu et al., 2015), MWF (Wu et al., 2006), PD (Mezer et al., 2013) and qMT (Levesque et al., 2010). Some metrics, however, are less stable on clinical setups and are adapted essentially for research scanners and studies; axon diameter measurements, for instance, present relatively large CoV values on clinical scanners (>11%) (Clayden et al., 2015) due to the requirement of strong gradients (Dyrby et al., 2012; Huang et al., 2015).

Particularly good whole-brain scan-rescan correlations (r >0.9) have been shown for the metrics *fr* (Tariq et al., 2012) and PD (Mezer et al., 2013). While such high values are quite remarkable, comparing correlation coefficients between quantitative metrics is particularly risky because r is highly dependent on the dynamic of the metric. For example, the g-ratio is relatively constant in healthy tissue, leading to low correlation coefficients. On the contrary, metrics that present high contrast between CSF and white matter would have high correlation coefficients as a result of CSF contamination. Also, the same metric can present very different correlation coefficients depending on the region of interest selected to perform the comparison (e.g. including both gray and white matter, as opposed to white matter only, usually improves the correlation coefficient). Future studies where several metrics are acquired within the same sample would shed light on this issue.

Another interesting metric that can be used to assess metric reproducibility is the intraclass correlation coefficient (ICC); indeed, the ICC shows the capability of a metric to detect differences between subjects that are significantly higher than the intra-subject scan-rescan difference. In the presence of significantly higher inter-subject differences, the ICC should be close to 1. Instead, if the values are similar, ICC will be close to 0.5. Using this statistic, it has been shown that both diffusion MRI (ICC=0.84 for *fr* in the spinal cord) (Grussu et al., 2015) and myelin imaging techniques (ICC=0.76 for MWF in the brain) (Meyers et al., 2013) are able to detect differences of white matter microstructure between two healthy subjects.

Sensitivity

Within the white matter, the microstructure can change drastically, mainly due to large differences in axon diameters between regions (see section “White matter microstructure”). While the white matter appears homogeneous on conventional MRI scans, quantitative MRI reveals microstructural differences, notably between different regions of the corpus callosum (Alexander et al., 2010; Barazany et al., 2009; Mezer et al., 2013; Stikov et al., 2015a) or between spinal cord tracts (Duval et al., 2015; Duval et al., 2016a; Fujiyoshi et al., 2016; Taso et al., 2016). These metrics can also track the microstructural changes related to brain development (Dean et al., 2016; MacMillan et al., 2011; Saito et al., 2012) or tissue deterioration in pathology (Chong et al., 2016; Fujiyoshi et al., 2016; Klawiter et al., 2011; Schmierer et al., 2008; Stikov et al., 2015a). The good sensitivity and reproducibility of these metrics suggest an improved capacity to detect subtle changes. Note that the sensitivity of quantitative MRI metrics implies the sensitivity of the non-quantitative MRI contrasts that produced this metric. However, compensating effects (e.g. simultaneous increase of T1 and MT) can conceal subtle changes in non-quantitative MRI contrast.

Specificity

Specificity is supposed to be the main asset of quantitative MRI metrics since these metrics disentangle the information from different sources. Unfortunately, assessing the specificity of quantitative MRI metrics is challenging due to the inter-correlation of many microstructural and MR parameters in the white matter (e.g. axon diameter, axon density, myelin content, water content, T1, T2*) (see the section “Challenges”). This issue can lead to incorrect interpretation of tissue structure: T1, for instance, has been considered successively as a semi-quantitative marker for myelin (Koenig et al., 1990), for water content (Fatouros and Marmarou, 1999), and even for axon diameter (Harkins et al., 2016). While the lack of specificity of the early quantitative MRI metrics is commonly pointed out (Alexander et al., 2007; Schwartz et al., 2005; Wheeler-Kingshott and Cercignani, 2009), model-based metrics bring new information (i.e. not perfectly correlated with conventional metrics) (Alexander et al., 2010; Zhang et al., 2012) that correlates with histology (Alexander et al., 2010; Barazany et al., 2009; Dula et al., 2010; Duval et al., 2015, 2016b; Ong and Wehrli, 2010; West et al., 2016b), and improves specificity in lesions (Kipp et al., 2016; Stikov et al., 2015a). More comprehensive models (Burcaw et al., 2015), as well as a new paradigm for measuring myelin (Sheth et al., 2016), should further improve the specificity of these metrics.

Accuracy

In the early stages of MRI biomarker development, accuracy could be considered a secondary issue. Indeed, if a quantitative metric presents good reproducibility across sites, as well as good sensitivity and specificity to microstructure integrity, this metric requires only normative values from healthy subjects in order to decide whether or not a patient presents abnormal values. An atlas of widely used semi-quantitative metrics has already been generated [e.g. FMRIB58_FA (Smith et al., 2004)].

However, accuracy is important in model-based quantitative MRI for validating the models and for allowing accurate interpretation of tissue integrity in different case scenarios. Accuracy is notably important when several metrics are combined, such as in computing the g-ratio, to prevent misinterpretation (Campbell et al., 2016). Accuracy is usually assessed by comparing MRI metrics with features extracted from *ex vivo* tissue such as those reported in figure 5. Some metrics can be directly compared such as PD, fr or axon diameter distribution. While PD and fr present relatively good accuracy (Nilsson et al., 2013; PS Tofts, 2003), axon diameter measurement has been reported to be over-

estimated by a factor of ~3 (Alexander et al., 2010; Horowitz et al., 2015; Innocenti et al., 2015; Zhang et al., 2011), and this was recently shown to be due to modeling issues (Burcaw et al., 2015) that were affecting the specificity of this metric. Unfortunately, many metrics, such as MWF and qMT, cannot be compared directly because they are specific to different microstructural features (myelin water for MWF, macromolecules for qMT). However, the MRI metric (e.g. MWF) can be calibrated to get accurate measurements of the microstructural feature (in this case, the myelin volume fraction, or MVF). Usually this calibration assumes a linear relationship between the MRI metric and the targeted microstructural parameter (i.e. MWF $\propto$ MVF), and is performed using synthetic phantoms (e.g. agar-agar solution with a known concentration) or using a few normative values measured with histology on healthy tissue (e.g. white matter and gray matter myelin content). While these calibration strategies might be a good approximation for healthy tissue, a linear assumption might not hold in pathology. For instance, how should we define the MWF or the *fr* in axons presenting unwrapped myelin sheaths? For these reasons, special care should be taken in evaluating the accuracy of quantitative MRI metrics.

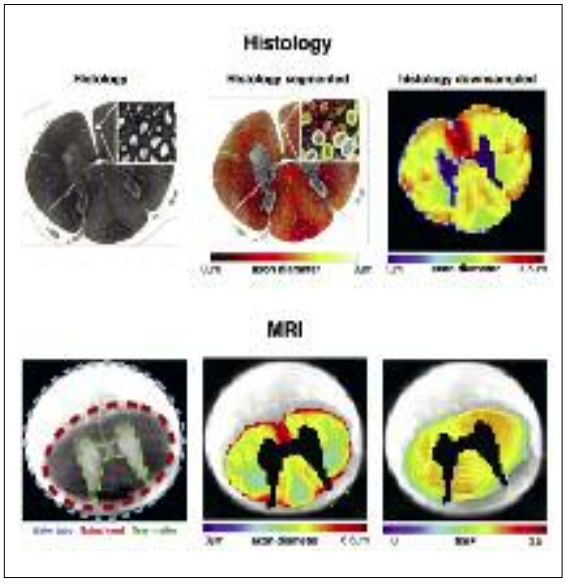

Figure 5 - A comparison of *ex vivo* quantitative MRI maps with histology.
Once segmented, histology can provide mean axon diameter or myelin volume fraction in a voxel. Visually, MRI and histology are in agreement, supporting the sensitivity of MRI to these specific microstructural properties.

Examples of quantitative MRI images

In this section, we present some examples of quantitative MRI maps. These maps are often easily distinguished from conventional MRI by the presence of a color bar associating a pixel color with a quantitative value. Figure 6 shows maps of MVF, axon volume fraction (AVF) and g-ratio obtained using qMT and NODDI on a multiple sclerosis patient. As shown in the section *Reproducibility*, the variation of these metrics across healthy subjects is relatively low (CoV<10%) which means that the underlying microstructure within a healthy population does not vary much. Knowing this, alteration of tissue integrity can be detected, not from the contrast with surrounding tissue, but directly from the quantitative value. Thanks to robust registration procedures, it is also possible to detect abnormal values automatically, segment a lesion, and provide statistics. Conventional fluid attenuated inversion recovery (FLAIR) contrast clearly indicates the presence of three hyperintense lesions. While these three lesions are associated with a reduction of myelin content MVF and axon density AVF, only one of them presents an abnormal g-ratio, suggesting a gain in specificity of the g-ratio metric. *Ex vivo* experiments, such as that presented in figure 5, enable comparison between MRI and histology to assess the sensitivity and accuracy of models. Because microstruc-

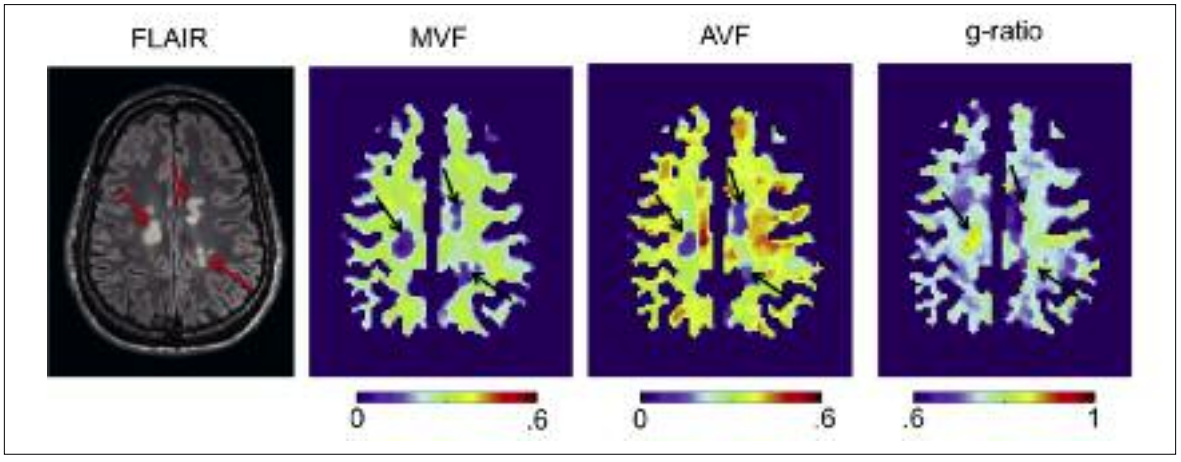

Figure 6 - Example of multi-parametric quantitative MRI maps of a multiple sclerosis patient.
Myelin volume fraction (MVF) was obtained using a qMT (Henkelman et al., 1993), axon volume fraction (AVF) was computed using the NODDI model (Zhang et al., 2012), and g-ratio was calculated from AVF and MVF (Stikov et al., 2015a). Conventional FLAIR contrast indicates the presence of three hyperintense lesions. These lesions are associated with a reduction in MVF and AVF, but only one lesion shows an abnormal g-ratio (>0.8).

tural parameters are correlated between each other (e.g. axon diameter, axon density and g-ratio), assessing their specificity is not straightforward, and would require a number of comparisons, not only in healthy white matter, but also in pathological tissue (West et al., 2016b).

Concluding remarks

In this brief review, we have described the most common quantitative MRI metrics and the methodology for modeling white matter. We showed that state-of-the-art quantitative MRI techniques produce reproducible maps that are highly sensitive to particular microstructural parameters. These maps are more specific to white matter microstructure than conventional MRI metrics, and can be calibrated to give meaningful numbers. While the long-term objective is to be able to retrieve the exact tissue microstructure and assess its integrity non-invasively, current quantitative MRI metrics should be interpreted carefully. With automatic processing pipelines, quantitative MRI should see more clinical applications in the next few years, notably for diagnosis and prognosis of diseases, as well as the monitoring of the effects of treatment.

Acknowledgments

We would like to thank Jennifer Campbell for her contribution to this presentation of an example dataset. This work was funded by the MS Society of Canada [EGID 2370], the Canada Research Chair in Quantitative Magnetic Resonance Imaging (JCA), the Canadian Institute of Health Research [CIHR FDN-143263], the Fonds de Recherche du Québec - Santé [28826], the Fonds de Recherche du Québec - Nature et Technologies [2015-PR-182754], the Natural Sciences and Engineering Research Council of Canada [435897-2013, 06774-2016], the Montreal Heart Foundation (NS) and the Quebec BioImaging Network (NS).

References

Adelman WJ Jr, Arnold JM, Gilbert DL (2013). Squid as Experimental Animals. New York, US, Springer.

Alexander DC, Hubbard PL, Hall MG, et al (2010). Orientationally invariant indices of axon diameter and density from diffusion MRI. Neuroimage 52:1374-1389.

Alexander DC (2008). A general framework for experiment design in diffusion MRI and its application in measuring direct tissue-microstructure features. Magn Reson Med 60:439-448.

Alexander AL, Lee JE, Lazar M, et al (2007). Diffusion tensor imaging of the brain. Neurotherapeutics 4:316-329.

Arciénega II, Brunet JF, Bloch J, et al (2010). Cell locations for AQP1, AQP4 and 9 in the non-human primate brain. Neuroscience 167:1103-1114.

Assaf Y, Basser PJ (2005). Composite hindered and restricted model of diffusion (CHARMED) MR imaging of the human brain. Neuroimage 27:48-58.

Assaf Y, Blumenfeld-Katzir T, Yovel Y, et al (2008). AxCaliber: a method for measuring axon diameter distribution from diffusion MRI. Magn Reson Med 59:1347-1354.

Avram L, Assaf Y, Cohen Y (2004). The effect of rotational angle and experimental parameters on the diffraction patterns and micro-structural information obtained from q-space diffusion NMR: implication for diffusion in white matter fibers. J Magn Reson 169:30-38.

Azevedo FAC, Carvalho LRB, Grinberg LT, et al (2009). Equal numbers of neuronal and nonneuronal cells make the human brain an isometrically scaled-up primate brain. J Comp Neurol 513:532-541.

Badaut J, Ashwal S, Adami A, et al (2011). Brain water mobility decreases after astrocytic aquaporin-4 inhibition using RNA interference. J Cereb Blood Flow Metab 31:819-831.

Barazany D, Basser PJ, Assaf Y (2009). In vivo measurement of axon diameter distribution in the corpus callosum of rat brain. Brain 132:1210-1220.

Baumann N, Pham-Dinh D (2001). Biology of oligodendrocyte and myelin in the mammalian central nervous system. Physiol Rev 81:871-927.

Biedenbach MA, De Vito JL, Brown AC (1986). Pyramidal tract of the cat: axon size and morphology. Exp Brain Res 61:303-310.

Bourne G (2012). The Structure and Function of Nervous Tissue, V2: Structure I. London, UK, Elsevier.

Burcaw LM, Fieremans E, Novikov DS (2015). Mesoscopic structure of neuronal tracts from time-dependent diffusion. Neuroimage 114:18-37.

Campbell JSW, Leppert IR, Boudreau M, et al (2016). Mapping the myelin g-ratio: promises and pitfalls. In: Proceedings of the 24th Annual Meeting of ISMRM. Singapore, p. 1501.

Chomiak T, Hu B (2009). What is the optimal value of the g-ratio for myelinated fibers in the rat CNS? A theoretical approach. PLoS One 4:e7754.

Chong AL, Chandra RV, Chuah KC, et al (2016). Proton density MRI increases detection of cervical spinal cord multiple sclerosis lesions compared with T2-weighted fast spin-echo. AJNR Am J Neuroradiol 37:180-184.

Clark CA, Le Bihan D (2000). Water diffusion compartmentation and anisotropy at high b values in the human brain. Magn Reson Med 44:852-859.

Clayden JD, Nagy Z, Weiskopf N, et al (2015). Microstructural parameter estimation in vivo using diffusion MRI and structured prior information. Magn Reson Med 75:1787-1796.

Cohen-Adad J, Wheeler-Kingshott C (2014). Quantitative MRI of the Spinal Cord. London, UK, Elsevier Science.

Daducci A, Canales-Rodríguez EJ, Zhang H, et al (2015). Accelerated Microstructure Imaging via Convex Optimization (AMICO) from diffusion MRI data. Neuroimage 105:32-44.

Dean DC 3rd, O'Muircheartaigh J, Dirks H, et al (2016). Mapping an index of the myelin g-ratio in infants using magnetic resonance imaging. Neuroimage 132:225-237.

Deoni SC, Rutt BK, Arun T, et al (2008). Gleaning multicomponent T1 and T2 information from steady-state imaging data. Magn Reson Med 60:1372-1387.

Deoni SC, Rutt BK, Peters TM (2003). Rapid combined T1 and T2 mapping using gradient recalled acquisition in the steady state. Magn Reson Med 49:515-526.

Dula AN, Gochberg DF, Valentine HL, et al (2010). Multiexponential T2, magnetization transfer, and quantitative histology in white matter tracts of rat spinal cord. Magn Reson Med 63: 902-909.

Duong TQ, Ackerman JJ, Ying HS, et al (1998). Evaluation of extra- and intracellular apparent diffusion in normal and globally ischemic rat brain via 19F NMR. Magn Reson Med 40:1-13.

Dupont SM, De Leener B, Taso M, et al (2016). Fully-integrated framework for the segmentation and registration of the spinal cord white and gray matter. Neuroimage doi: 10.1016/j.neuroimage.2016.09.026.

Duval T, Lévy S, Stikov N, et al (2016a). g-Ratio weighted imaging of the human spinal cord in vivo. Neuroimage doi: 10.1016/j.neuroimage.2016.09.018.

Duval T, Perraud B, Vuong M-T, et al (2016b). Validation of quantitative MRI metrics using full slice histology with automatic axon segmentation. In: Proceedings of the 24th Annual Meeting of ISMRM. Singapore, p. 928.

Duval T, McNab JA, Setsompop K, et al (2015). In vivo mapping of human spinal cord microstructure at 300mT/m. Neuroimage 118:494-507.

Dyrby TB, Søgaard LV, Hall MG, et al (2012). Contrast and stability of the axon diameter index from microstructure imaging with diffusion MRI. Magn Reson Med 70:711-721.

Einstein A (1956). Investigations on the Theory of the Brownian Movement. Dover Books on Physics Series. Mineola, Dover Publications.

Fatouros PP, Marmarou A (1999). Use of magnetic resonance imaging for in vivo measurements of water content in human brain: method and normal values. J Neurosurg 90:109-115.

Ferizi U, Schneider T, Witzel T, et al (2015). White matter compartment models for in vivo diffusion MRI at 300mT/m. Neuroimage 118:468-483.

Ferizi U, Schneider T, Panagiotaki E, et al (2014). A ranking of diffusion MRI compartment models with in vivo human brain data. Magn Reson Med 72:1785-1792.

Fields RD (2008). White matter in learning, cognition and psychiatric disorders. Trends Neurosci 31:361-370.

FitzGibbon T, Nestorovski Z (2013). Human intraretinal myelination: axon diameters and axon/myelin thickness ratios. Indian J Ophthalmol 61:567-575.

Fujiyoshi K, Hikishima K, Nakahara J, et al (2016). Application of q-Space diffusion MRI for the visualization of white matter. J Neurosci 36:2796-2808.

Giuliodori MJ, DiCarlo SE (2004). Myelinated vs. unmyelinated nerve conduction: a novel way of understanding the mechanisms. Adv Physiol Educ 28: 80-81.

Grussu F, Schneider T, Yates RL, et al (2016). A framework for optimal whole-sample histological quantification of neurite orientation dispersion in the human spinal cord. J. Neurosci Methods 273:20-32.

Grussu F, Schneider T, Zhang H, et al (2015). Neurite orientation dispersion and density imaging of the healthy cervical spinal cord in vivo. Neuroimage 111:590-601.

Harkins KD, Xu J, Dula AN, et al (2016). The microstructural correlates of T1 in white matter. Magn Reson Med 75:1341-1345.

Harrison R, Bronskill MJ, Henkelman RM (1995). Magnetization transfer and T2 relaxation components in tissue. Magn Reson Med 33:490-496.

Helms G, Dathe H, Kallenberg K, et al (2008). High-resolution maps of magnetization transfer with inherent correction for RF inhomogeneity and T1 relaxation obtained from 3D FLASH MRI. Magn Reson Med 60:1396-1407.

Henkelman RM, Stanisz GJ, Graham SJ (2001). Magnetization transfer in MRI: a review. NMR Biomed 14:57-64.

Henkelman RM, Huang X, Xiang QS, et al (1993). Quantitative interpretation of magnetization transfer. Magn Reson Med 29:759-766.

Herculano-Houzel S (2014). The glia/neuron ratio: how it varies uniformly across brain structures and species and what that means for brain physiology and evolution. Glia 62:1377-1391.

Horowitz A, Barazany D, Tavor I, et al (2015). In vivo correlation between axon diameter and conduction velocity in the human brain. Brain Struct. Funct 220:1777-1788.

Huang SY, Nummenmaa A, Witzel T, et al (2015). The impact of gradient strength on in vivo diffusion MRI estimates of axon diameter. Neuroimage 106:464-472.

Innocenti GM, Caminiti R, Aboitiz F (2015). Comments on the paper by Horowitz et al. (2014). Brain Struct Funct 220:1789-1790.

Johansen-Berg H, Behrens TEJ (2013). Diffusion MRI: From Quantitative Measurement to In vivo Neuroanatomy. London, Elsevier Science.

Kipp L, Cawley N, Prados F, et al (2016). Neurite Orientation Dispersion and Density Imaging (NODDI) in RRMS. In: (Proceedings) 31st Congress of the European Committee for Treatment and Research in Multiple Sclerosis (ECTRIMS). Barcelona, p. 9.

Klawiter EC, Schmidt RE, Trinkaus K, et al (2011). Radial diffusivity predicts demyelination in ex vivo multiple sclerosis spinal cords. Neuroimage 55:1454-1460.

Koenig SH, Brown RD 3rd, Spiller M, et al (1990). Relaxometry of brain: why white matter appears bright in MRI. Magn Reson Med 14:482-495.

Lajtha A (2013). Pathological Neurochemistry. New York, NY, US, Springer.

Levesque IR, Pike GB (2009). Characterizing healthy and diseased white matter using quantitative magnetization transfer and multicomponent T2 relaxometry: a unified view via a four-pool model. Magn Reson Med 62:1487-1496.

Levesque IR, Sled JG, Narayanan S, et al (2010). Reproducibility of quantitative magnetization-transfer imaging parameters from repeated measurements. Magn Reson Med 64:391-400.

Liewald D, Miller R, Logothetis N, et al (2014). Distribution of axon diameters in cortical white matter: an electron-microscopic study on three human brains and a macaque. Biol Cybern 108:541-557.

Lundell H, Sønderby CK, Dyrby TB (2015). Diffusion weighted imaging with circularly polarized oscillating gradients. Magn Reson Med 73:1171-1176.

MacKay A, Whittall K, Adler J, et al (1994). In vivo visualization of myelin water in brain by magnetic resonance. Magn Reson Med 31:673-677.

MacMillan EL, Mädler B, Fichtner N, et al (2011). Myelin water and T(2) relaxation measurements in the healthy cervical spinal cord at 3.0T: repeatability and changes with age. Neuroimage 54:1083-1090.

Ma D, Gulani V, Seiberlich N, et al (2013). Magnetic resonance fingerprinting. Nature 495:187-192.

Marques JP, Kober T, Krueger G, et al (2010). MP2RAGE, a self bias-field corrected sequence for improved segmentation and T1-mapping at high field. Neuroimage 49: 1271-1281.

Meier C, Dreher W, Leibfritz D (2003). Diffusion in compartmental systems. II. Diffusion-weighted measurements of rat brain tissue in vivo and postmortem at very large b-values. Magn Reson Med 50: 510-514.

Meyers SM, Vavasour IM, Mädler B, et al (2013). Multicenter measurements of myelin water fraction and geometric mean T2 : intra- and intersite reproducibility. J Magn Reson Imaging 38:1445-1453.

Mezer A, Yeatman JD, Stikov N, et al (2013). Quantifying the local tissue volume and composition in individual brains with magnetic resonance imaging. Nat Med 19:1667-1672.

Morell P, Quarles RH (1999). Myelin Formation, Structure and Biochemistry. Philadelphia, PA, Lippincott-Raven, Chapter 4.

Mottershead JP, Schmierer K, Clemence M, et al (2003). High field MRI correlates of myelin content and axonal density in multiple sclerosis--a post-mortem study of the spinal cord. J Neurol 250:1293-1301.

Nielsen S, Nagelhus EA, Amiry-Moghaddam M, et al (1997). Specialized membrane domains for water transport in glial cells: high-resolution immunogold cytochemistry of aquaporin-4 in rat brain. J Neurosci 17:171-180.

Nisson M, van Western D, Ståhlberg F, et al (2013). The role of tissue microstructure and water exchange in biophysical modelling of diffusion in white matter. MAGMA 26:345-370.

Nilsson M, Lätt J, Ståhlberg F, et al (2012). The importance of axonal undulation in diffusion MR measurements: a Monte Carlo simulation study. NMR Biomed 24:279-805.

Norton WT, Cammer W (1984). Isolation and characterization of myelin. In: Morell P (Ed), Myelin. Boston, Springer US, pp. 147-195.

Norton WT, Autilio LA (1966). The lipid composition of purified bovine brain myelin. J Neurochem 13: 213-222.

O'Brien JS, Sampson EL (1965). Lipid composition of the normal human brain: gray matter, white matter, and myelin. J Lipid Res 6:537-544.

Oh SH, Bilello M, Schindler M, et al (2013). Direct visualization of short transverse relaxation time component (ViSTa). Neuroimage 83:485-492.

Ong HH, Wehrli FW (2010). Quantifying axon diameter and intra-cellular volume fraction in excised mouse spinal cord with q-space imaging. Neuroimage 51:1360-1366.

Panagiotaki E, Schneider T, Siow B, et al (2012). Compartment models of the diffusion MR signal in brain white matter: a taxonomy and comparison. Neuroimage 59:2241-2254.

Perge JA, Koch K, Miller R, et al (2009). How the optic nerve allocates space, energy capacity, and information. J Neurosci 29: 7917-7928.

Prasloski T, Rauscher A, MacKay AL, et al (2012). Rapid whole cerebrum myelin water imaging using a 3D GRASE sequence. Neuroimage 63:533-539.

Rovira A, Auger C, Alonso J (2013). Magnetic resonance monitoring of lesion evolution in multiple sclerosis. Ther Adv Neurol Disord 6:298-310.

Saito N, Watanabe M, Sakai O, et al (2012). Human lifespan age-related changes of the brain proton density by quantitative MRI. In: Proceedings of the 20th Annual Meeting of ISMRM. Melbourne, p. 780.

Schmierer K, Scaravilli F, Altmann DR, et al (2004). Magnetization transfer ratio and myelin in postmortem multiple sclerosis brain. Ann Neurol 56:407-415.

Schmierer K, Wheeler-Kingshott CA, Tozer DJ, et al (2008). Quantitative magnetic resonance of postmortem multiple sclerosis brain before and after fixation. Magn Reson Med 59:268-277.

Schwartz ED, Duda J, Shumsky JS, et al (2005). Spinal cord diffusion tensor imaging and fiber tracking can identify white matter tract disruption and glial scar orientation following lateral funiculotomy. J Neurotrauma 22:1388-1398.

Sepehrband F, Alexander DC, Kurniawan ND, et al (2016). Towards higher sensitivity and stability of axon diameter estimation with diffusion-weighted MRI. NMR Biomed 29:293-308.

Shemesh N, Álvarez GA, Frydman L (2015). Size Distribution Imaging by Non-Uniform Oscillating-Gradient Spin Echo (NOGSE) MRI. PLoS One 10: e0133201.

Shepherd VA (2006). The cytomatrix as a cooperative system of macromolecular and water networks. Curr Top Dev Biol 75:171-223.

Sheth V, Shao H, Chen J, et al (2016). Magnetic resonance imaging of myelin using ultrashort Echo time (UTE) pulse sequences: phantom, specimen, volunteer and multiple sclerosis patient studies. Neuroimage 136:37-44.

Smith SM, Jenkinson M, Woolrich MW, et al (2004). Advances in functional and structural MR image analysis and implementation as FSL. Neuroimage 23 Suppl 1: S208-219.

Stejskal EO, Tanner JE (1965). Spin diffusion measurements: spin echoes in the presence of a time-dependent field gradient. The Journal of Chemical Physics 42:288-292.

Stikov N, Campbell JS, Stroh T, et al (2015a). Quantitative analysis of the myelin g-ratio from electron microscopy images of the macaque corpus callosum. Data Brief 4:368-373.

Stikov N, Campbell JS, Stroh T, et al (2015b). In vivo histology of the myelin g-ratio with magnetic resonance imaging. Neuroimage 118:397-405.

Stüber C, Morawski M, Schäfer A, et al. (2014). Myelin and iron concentration in the human brain: a quantitative study of MRI contrast. Neuroimage 93 Pt 1:95-106.

Syková E, Nicholson C (2008). Diffusion in brain extracellular space. Physiol Rev 88: 1277-1340.

Syková E, Vargová L, Prokopová S, et al (1999). Glial swelling and astrogliosis produce diffusion barriers in the rat spinal cord. Glia 25:56-70.

Tariq M, Schneider T, Alexander DC, et al (2012). Scan-rescan reproducibility of neurite microstructure estimates using NODDI. In: Xie X (Ed) Medical Image Understanding and Analysis 2012: Proceedings of the 16th Conference on Medical Image Understanding and Analysis. Swansea, UK, pp. 255-261.

Taso M, Girard OM, Duhamel G, et al (2016). Tract-specific and age-related variations of the spinal cord microstructure: a multi-parametric MRI study using diffusion tensor imaging (DTI) and inhomogeneous magnetization transfer (ihMT). NMR Biomed 29:817-832.

Tofts P (2003). Quantitative MRI of the Brain: Measuring Changes Caused by Disease. Chichester, UK, John Wiley & Sons.

Tofts PS (2003). PD: proton density of tissue water. In: Tofts P (Ed), Quantitative MRI of the brain. Chichester, UK, John Wiley & Sons, pp. 85-109.

Van AT, Holdsworth SJ, Bammer R (2014). In vivo investigation of restricted diffusion in the human brain with optimized oscillating diffusion gradient encoding. Magn Reson Med 71:83-94.

Vollmar C, O'Muircheartaigh J, Barker GJ, et al (2010). Identical, but not the same: intra-site and inter-site reproducibility of fractional anisotropy measures on two 3.0T scanners. Neuroimage 51: 1384-1394.

Volz S, Nöth U, Deichmann R (2012). Correction of systematic errors in quantitative proton density mapping. Magn Reson Med 68:74-85.

Wang LZ, Caprihan A, Fukushima E (1995). The Narrow-Pulse Criterion for Pulsed-Gradient Spin-Echo Diffusion Measurements. J Magn Reson A 117:209-219.

West KL, Kelm ND, Carson RP, et al (2016a). A revised model for estimating g-ratio from MRI. Neuroimage 125:1155-1158.

West KL, Kelm ND, Gochberg DF, et al (2016b). Quantitative estimates of myelin volume fraction from T2 and magnetization transfer. In: Proceedings of the 24th Annual Meeting of ISMRM, Singapore, p. 1277.

Wheeler-Kingshott CA, Cercignani M (2009). About "axial" and "radial" diffusivities. Magn Reson Med 61:1255-1260.

Wolff SD, Balaban RS (1989). Magnetization transfer contrast (MTC) and tissue water proton relaxation in vivo. Magn Reson Med 10: 135-144.

Wu Y, Alexander AL, Fleming JO, et al (2006). Myelin water fraction in human cervical spinal cord in vivo. J Comput Assist Tomogr 30: 304-306.

Zaimi A, Duval T, Gasecka A, et al (2016). AxonSeg: open source software for axon and myelin segmentation and morphometric analysis. Front Neuroinform 10:37.

Zhang H, Hubbard PL, Parker GJM, et al (2011). Axon diameter mapping in the presence of orientation dispersion with diffusion MRI. Neuroimage 56: 1301-1315.

Zhang H, Schneider T, Wheeler-Kingshott CA, et al. (2012). NODDI: practical in vivo neurite orientation dispersion and density imaging of the human brain. Neuroimage 61: 1000-1016.